COMPARISON OF A TURBULENT BOUNDARY LAYER ENCOUNTERING A RAMP VERSUS A BUMP

Akhileshwar Borra
Department of Aerospace Engineering
University of Illinois Urbana-Champaign
104 S. Wright St., Urbana, IL 61801
aborra2@illinois.edu

Theresa Saxton-Fox
Department of Aerospace Engineering
University of Illinois Urbana-Champaign
104 S. Wright St., Urbana, IL 61801
tsaxtonf@illinois.edu

ABSTRACT

The statistics of a turbulent boundary layer experiencing different spatially varying pressure gradient histories were evaluated experimentally. Two separate sets of experiments were conducted with a bump and a downstream facing ramp downstream of a flat plate. The geometry of the second half of the bump and the ramp are similar, isolating the effect of curvature in the separating region. The bump imposed a series of pressure gradients: a mild adverse pressure gradient (APG), strong favorable pressure gradient (FPG), strong APG, and a recovery region. Meanwhile, the ramp imposed a mild FPG from the leading edge of the plate, a moderate FPG directly ahead of the ramp, a strong APG and a recovery region. Time-resolved particle image velocimetry and static pressure measurements were collected across the entire ramp and bump surface. In this work, the pressure gradient imposed will be characterized using the static pressure measurements. The mean streamwise velocity and the backflow percentage are compared on the flat plate, and on the bump and ramp. The streamwise mean velocity results for the bump shows the growth of the boundary layer on the flat plate in a zero pressure gradient environment, followed by a deceleration due to a mild APG at the leading edge of the bump. Then, for the remainder of the upstream half of the bump, the TBL encountered a strong FPG which accelerated the TBL. In contrast for the ramp, the TBL is influenced by the presence of a weak FPG starting at the leading edge of the flat plate. Upstream of the start of the downward facing ramp, the TBL is accelerated due to a mild FPG. The different pressure gradients upstream of the strong APG region for both geometries leads to different inflow conditions into the strong APG region. This results in a similar separation behavior in the strong APG region for the bump and the downward facing ramp however with a delayed separation and reattachment point for the ramp.

Introduction

In many engineering applications, turbulent boundary layers encounter complex spatially varying pressure gradients that can alter the state and behavior of the TBL. These complicated spatially varying pressure gradients can include any combination and order of zero, favorable and adverse pressure gradients. Different combinations of pressure gradients will result in varied states of the boundary layer and will have a considerable impact on the fluid-dynamic forces of importance, such as drag. Understanding the effects of pressure gradients can lead to more efficient drag reduction methods and separation control. However, lower-fidelity modeling approaches, such as RANS, wall-modeled LES and wall-resolved LES, have failed at accurately predicting important characteristics such as coefficient of friction, C_f, and the location of separation (Balin, 2016). Uzun & Malik (2022) showed that for matched pressure gradients, RANS over predicts C_f in an FPG region and under predicts the separated region compared to a DNS simulation.

A FPG accelerates the external flow and results in an enlarged viscous sublayer and buffer region and a smaller wake region in the mean flow normalized in inner units (Bourassa & Thomas, 2009). For strong FPGs, defined as $0.5 \times 10^{-6} < K < 6 \times 10^{-6}$, where K is the acceleration parameter, the presence of the logarithm region is still debated (Dixit & Ramesh, 2010; Badri Narayanan & Ramjee, 1969). The acceleration parameter is defined as $K = \frac{\nu}{U^2}\frac{dU}{dX}$, where ν is the kinematic viscosity and U is the streamwise velocity. Near-wall streaks have been observed to elongate in the streamwise direction and reduce in intensity (Kline *et al.*, 1967). The FPG drives a decay in the Reynolds stresses, which is more pronounced in the outer region (Volino, 2020; Bourassa & Thomas, 2009). This decay in the Reynolds stresses has been connected to the behavior of large scales present in the TBL. The large scales tend to decrease in energy, elongate in the streamwise direction and become less inclined as a favorable pressure gradient increases (Dixit & Ramesh, 2010). In some cases where the favorable pressure gradient is strong enough, the process of relaminarization of the boundary layer has been observed. Relaminarization is a gradual process accompanied by significant alterations to the boundary layer's structure. This process involves the thinning of the boundary layer, deviations from the established law of the wall and law of the wake, a change to the shape factor and changes in skin-friction characteristics

(Sreenivasan, 1982).

In contrast, an APG decelerates the external flow and results in a thinner viscous sublayer and buffer region with a larger wake region in the mean flow normalized in inner units (Nagano & Tagawa, 1993). Similar to FPGs, the existence of the log law is still debated for APG TBLs. As the adverse pressure gradient strength increases, the streamwise Reynolds stress profile exhibits an outer peak, which has been related to the increase in the activity of the large scales in the outer region (Monty *et al.*, 2011). The strengthening of the outer peak in Reynolds stresses has been connected with an increase in turbulent production. In turbulent spectra, the outer peak is centered around a streamwise wavelength of 3δ and location at $y \equiv 0.2 - 0.5\delta$ (Vila *et al.*, 2020). The inner peak has also been shown to strengthen due to an adverse pressure gradient. Near-wall streaks tend to get shorter and increase in intensity when an adverse pressure gradient is encountered (Kline *et al.*, 1967). With a strong enough adverse pressure gradient, separation of the boundary layer with large regions of back flow is possible. In his seminal review of turbulent boundary layer separation, Simpson (1989) categorizes the state of separation based on the fraction of time the flow moves downstream, γ, as follows: incipient detachment (ID) with instantaneous backflow 1% of the time, intermittent transitory detachment with instantaneous backflow 20% of the time, transitory detachment with instantaneous back flow 50% of the time and detachment occurs where the time-average wall shear stress is 0. Separation leads to a thickening of the boundary layer with a region of rotational flow and a large increase in the wall-normal velocity. Na & Moin (1998) performed DNS using suction and blowing to impose pressure gradients and identified that turbulent structures move away from the wall as they approach the separated region. Then, the structures move into the shear layer, turn around the separation bubble and reapproach the wall in the reattachment region. The authors also identified that the large-scale structures grow in the shear layer and, in some instances, merge. Many authors have shown the instantaneous detachment and reattachment points of the separated boundary layer are not fixed in time but rather fluctuate significantly upstream and downstream (Patrick, 1987; Wu *et al.*, 2020).

Although understanding isolated adverse or favorable pressure gradients is important, in many applications of interest, a series of varying strengths and types of pressure gradients are present. Previous studies have shown the history or evolution of the pressure gradient will affect the behavior and state of the TBL (Vinuesa *et al.*, 2017). TBLs experiencing both an adverse and favorable pressure gradient in sequence have been studied since the work of Baskaran *et al.* (1987) and Webster *et al.* (1996). The authors studied the behavior of a boundary layer over a bump or hill with various boundary layer thickness to height ratios. In sequential favorable and adverse pressure TBLs, the boundary layer can behave differently than a purely adverse or favorable pressure gradient. For a strong enough FPG upstream of an APG, the process of relaminarization can begin, which alters the state of the boundary layer prior to the impact of the APG. The relaminarized boundary layer can be more resilient to the strong APG and can delay the onset of separation (Balin & Jansen, 2021). Previous researchers have found the formation of an internal layer to be triggered in these flows due to surface curvature discontinuity, change in sign of pressure gradient or even a change in the strength of a pressure gradient (Baskaran *et al.*, 1987; Parthasarathy, 2023). The internal layer can cause the inner and outer region to behave independently of each other. The flow in the inner region is largely driven only by the pressure gradient while the outer region is impacted by the pressure gradient and streamline curvature (Balin & Jansen, 2021).

Along with the influence of pressure gradients, it is also important to consider the impacts of curvature on the state of the boundary layer. Concave curvatures increase the Reynolds shear stress and the wall-normal transport of momentum. They also reduce the wake of the streamwise velocity (So, 1975). Convex curvatures, which usually have the opposite effects, reduce the Reynolds shear stress and can even make the Reynolds shear stress change signs. Furthermore, they can drastically reduce the turbulent kinetic energy away from the wall, reduce the extent of the log law and increase the wake (So & Mellor, 1973). When studying boundary layers under the effects of both pressure gradients and wall curvature, it is important to understand the mechanism that is more dominant.

In summary, previous works regarding the behavior of TBLs under pressure gradients and curvature effects have provided insight into some of the changes that can be brought upon due to the PGs. However, there are still many aspects of these interactions and changes to the TBL that are unknown. Due to the relevance of pressure gradients in many applications and the lack of accuracy in low- and medium-fidelity computational methods to capture the behavior of these PG TBLs, there remains an interest to further study PGs TBLs experimentally. In this context, in its CFD Vision 2030, NASA highlighted "smooth body separation remains very hard to simulate accurately and efficiently... In general, two critical components of flow physics need to be modeled accurately: the exact location of separation as controlled by boundary-layer physics and the feedback from the separation region to the boundary layer" (Slotnick *et al.*, 2014). To support the efforts in the turbulence community, the goal of this work is to evaluate the effect of the pressure gradient history by comparing the state of the boundary layers under the influence two different spatially varying pressure gradients.

Experimental Methods

Experiments were performed in the Turbulent Boundary Layer wind tunnel (TBLWT) at the University of Illinois Urbana-Champaign. TBLWT has a contraction ratio of 27:1 and a test section of 38.1 cm by 38.1 cm. The tunnel is capable of reaching speeds of 25 m/s with a turbulence intensity of approximately 0.5%. The boundary layer was tripped using sandpaper at the leading edge of the flat plate and allowed to develop for 2.46 m for the bump and 2.69 m for the ramp. The bump geometry, inspired by the Boeing bump (Prakash *et al.*, 2022; Gray *et al.*, 2023; Uzun & Malik, 2022), is defined by

$$y(x) = \frac{h}{2} exp(-(x/x_0)^2) \tag{1}$$

where $h = 0.15L_T$, $x_0 = 0.225L_T$ and L_T is the height of the wind tunnel, which is 38.1 cm. Schematics of the bump and ramp are shown in figure 1. The bump and the ramp were 3D printed using PLA and then sanded on top to create a smooth surface. Data was collected for both the bump and ramp at incoming flow speeds of 7.5, 10 and 15 m/s.

Velocity fields were obtained using particle image velocimetry (PIV) by using two adjacent cameras in the streamwise - wall-normal plane. The upstream camera had a field of view of 5.625" in the streamwise direction and 3.52" in the wall-normal direction while the other camera had an FOV of 4.5" in both directions. Data collection from these cameras

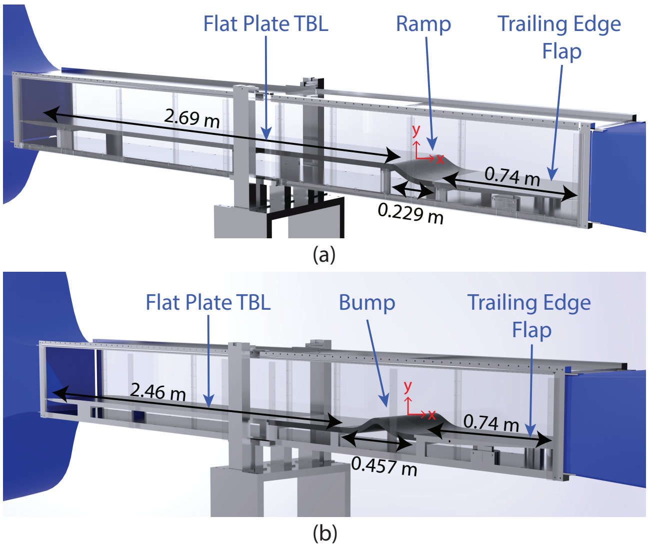

Figure 1. Experimental setup of turbulent boundary layer wind tunnel with (a) ramp and (b) bump

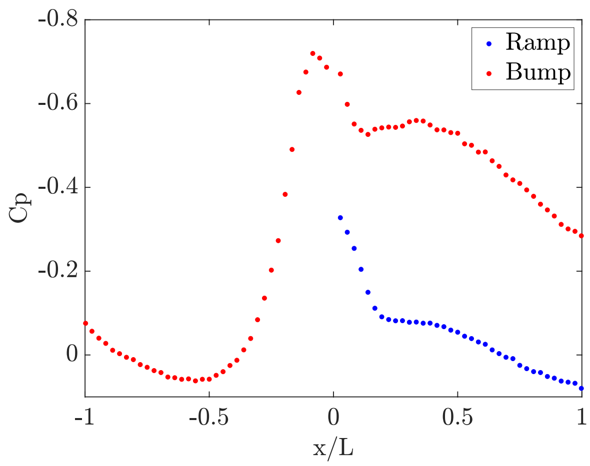

Figure 2. C_p distribution for the bump in red and ramp in blue

occurred simultaneously, and collected at frequencies of 100 Hz and 3750 Hz. For the bump, three separate sets of PIV data were acquired: on the flat plate region of the bump, the upstream half of the bump and downstream half of the bump. For the ramp, two separates sets of PIV data were collected: on the flat plate upstream of the ramp and the downward facing ramp. A Phantom VEO 710 and Photron Fastcam S5000 were used for the PIV collection along with a Terra 572-80 PIV laser. The velocity fields were calculated using DaVis software. Surface pressure measurements were also acquired through pressure ports in the 3D printed geometry using an Initium pressure scanning system with 10 in-WC blocks.

The pressure distribution for the ramp and bump as measured by the surface pressure measurements are displayed in figure 2. The coordinate system in the streamwise direction is defined such that the beginning of the ramp is $x/L = 0$ and the apex of the bump is $x/L = 0$, where L is the length of the ramp or half the length of the bump. The pressure distribution is plotted as the coefficient of pressure C_p where $C_p = \frac{P-P_\infty}{\frac{1}{2}\rho V_\infty}$. P_∞ is measured on the windows near the leading edge of the flat plate and V_∞ is defined as the freestream velocity on the flat plate. The C_p measurement at the leading edge of the bump was near 0 indicating the turbulent boundary layer grows in a near zero pressure gradient on the flat plate. The increase in the C_p distribution from $x/L = -1$ to $x/L = -0.55$ indicated the presence of an adverse pressure gradient. From $x/L = -0.55$ to $x/L = 0$, the pressure increased from 0.06 to -0.72 indicating the presence of a strong FPG. Following the FPG, the C_p decreased from -0.72 to -0.52 indicated a strong APG until $x/L = 0.13$. The C_p stagnates at $x/L = 0.13$ indicating flow separation has occurred. At the trailing edge of the bump, the pressure continues to recover however the recovery is not completed on the surface of the ramp. In contrast for the ramp, the first C_p measurement plotted in blue in figure 2 starts at -0.68 indicating the presence of a FPG starting at the leading edge of the flat plate. From $x/L = 0.02$ to $x/L = 0.25$, the C_p increases due to the presence of a strong APG. The C_p stagnates at this location indicating a separated TBL. At the trailing edge the ramp, the pressure fully recovers to $C_p = 0$. Comparing the pressure gradients imposed by both surfaces, the C_p measurements show different pressure gradient histories for the two geometries. Although there was an FPG present for the ramp starting at the leading edge of the flat plate, the bump imposed a much stronger FPG due to the upstream half of the bump. However, the mild FPG ahead of the ramp was present for a much longer spatial extent. The strength of the pressure gradient defined by the Clauser pressure gradient parameter, β, peaked in the strong FPG region of the bump at -7.65 at a location of $x/L = -0.16$ and in the strong APG region of the bump at 4.7 at a location of $x/L = 0.02$. In contrast, the APG for the ramp peaked at 2.72 at a location of $x/L = 0.11$. The Clauser pressure gradient parameter is typically defined as $\beta = \delta^*/u_\tau dP_e/dx$, where δ^* is the displacement thickness, u_τ is the friction velocity and dP_e/dx is the pressure gradient at the edge of the boundary layer. However, due to the lack of wall shear stress measurements in the regions with the pressure gradient, u_τ from the flat plate region calculated using the Clauser method was used to calculate β at all locations.

Results and Discussion

The response of the TBL to the imposed pressure gradients is evaluated using the particle image velocimetry data over the ramp, bump and the flat plate ahead of both geometries for the 10 m/s case. The mean streamwise velocity over

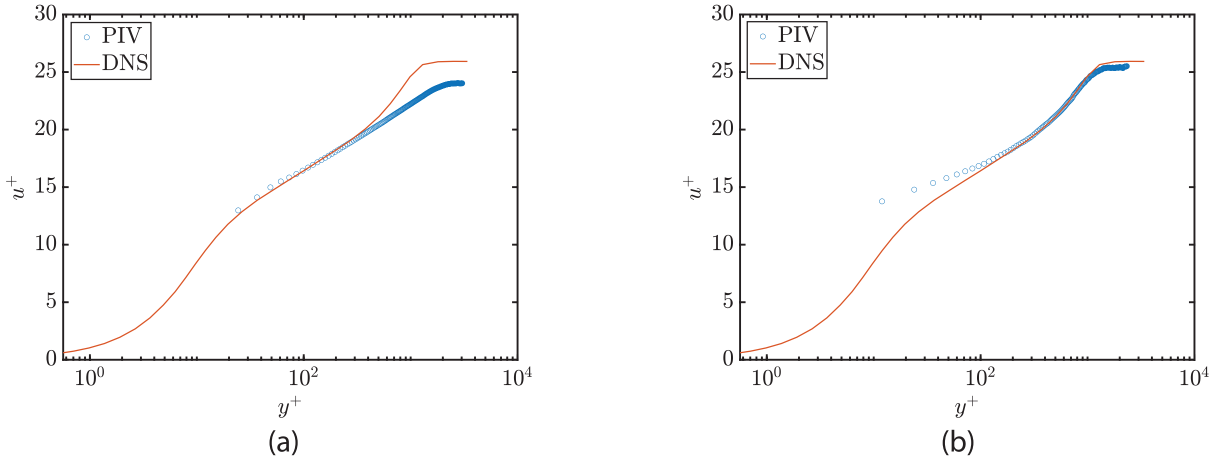

Figure 3. Mean streamwise velocity normalized in inner units on the flat plate ahead of the (a) ramp and (b) bump geometries

the ramp, bump and on the flat plate region ahead of both geometries is discussed in this paper as well as the backflow perctage in the strong APG regions where the TBL has separated. The x and y axes are normalized using the boundary layer thickness, δ. The mean and backflow percentages are evaluated in a coordinate system perpendicular to the local curvature at each of the streamwise locations over the surface of the bump and ramp and denoted as $\hat{n}$. The boundary layer edge parameters, such as boundary layer thickness and edge velocity, are identified using the diagnostic plot method (Vineusa *et al.*, 2016) for the locations where the TBL is impacted by the PGs. For the data on the flat plate, the edge parameters are evaluated based on the location of the velocity being 99% of the freestream velocity. The Reynolds number at the upstream edge of the bump based on the distance from the leading edge was $Re_L = 1.67 \times 10^6$, while the momentum based Reynolds number was $Re_\theta = 4425$ and the friction based Reynolds number was $Re_\tau = 1340$. In contrast, the respective Reynolds numbers at the upstream edge of the ramp were $Re_L = 1.83 \times 10^6$, $Re_\theta = 4382$ and $Re_\tau = 1830$. The boundary layer thickness, δ_{99}, at the upstream edge of the bump and ramp was 55 mm and 74 mm respectively. The state of the incoming boundary layer into the bump and ramp are shown through inner scaled streamwise mean velocity in Figure 3 as blue circles and data from a direct numerical simulation performed by Schlatter & Orlu (2010) at a similar Re_θ are shown with an orange line. The inner scaled mean velocity data for the ramp, shown in figure 3a, shows agreement in the logarithmic region; however, the wake has been weakened. A weakening of the wake indicates that a favorable pressure gradient on the boundary layer started well upstream of the start of the ramp. Ahead of the bump, the inner scaled mean streamwise velocity, shown in figure 3b, matched well with the DNS data in the logarithmic and the wake region. This implies that the turbulent boundary layer upstream of the bump developed in a zero pressure gradient. The turbulent boundary layers have experienced different PG histories before start of the bump and the ramp, changing the inflow conditions into the geometries. We are interested in how these different boundary layers respond to the similar curvature and geometric conditions on the second half of the bump and the ramp.

The spatial evolution of the TBL is evaluated through the outer scaled mean streamwise velocity at various locations in figure 4. The outer scaled mean streamwise velocities for the flat plate ahead of the bump, upstream and downstream half of the bumps are shown in figures 4a, b and c respectively. In figures 4d and e, the outer scaled mean velocity is shown for the flat plate ahead of the ramp and on the ramp surface respectively. For all of the streamwise velocity and backflow percentage figures, the earliest location in each region is plotted in blue with a gradient to red for the last location in the respective region. The mean streamwise velocity profiles on the flat plate upstream of the bump (Figure 4a) show minor variations across the field of view, with the profile becoming less full as the flow reaches the beginning of the bump. The profiles become less full due to the influence of an adverse pressure gradient upstream of the bump. In Figure 4b, profiles at 7 locations on the upstream half of the bump surface are shown. The velocity profile continues to become less full and decelerate initially, at locations $x/L = -0.95$, $x/L = -0.8$ and $x/L = -0.65$. The profiles then start to become fuller as seen in $x/L = -0.5$, $x/L = -0.2$ and $x/L = -0.15$. Note that the velocity profiles at $x/L = -0.15$ are fuller than the ones at $x/L = -0.95$, indicating that the FPG on the upstream half of the bump ultimately accelerates the boundary layer more than the initial deceleration imposed by the APG. In figure 4c, seven velocity profiles normal to the surface on the downstream half of the bump are shown. Some flow separation is already observed at $x/L = 0.15$, the earliest location evaluated, seen as a slightly negative mean velocity value near the wall. From $x/L = 0.25$ to $x/L = 0.5$, the magnitude of the mean reverse flow and the wall-normal extent of the reverse flow increases. The flow starts to accelerate and the magnitude of the reverse flow decreases from $x/L = 0.5$ to $x/L = 0.65$ where the flow is close to reattachment. Positions after $x/L = 0.65$ contained no reverse flow suggesting the flow has reattached. An inflection point is present.

The mean velocity profiles on the flat plate ahead of the ramp is shown in figure 4d and on the ramp surface in figure 4e. Upstream of the ramp, on the flat plate, the turbulent boundary layer encountered a mild favorable pressure gradient which resulted in a further acceleration of the flow. This is evident due to the profile becoming fuller from a streamwise location of $x/L = -0.5$, shown in blue in 4e, to $x/L = -0.15$, shown in red. The velocity profiles normal to the surface on the downstream facing ramp are shown in Figure 4e. Initially, the flow continues to accelerate; the profile at $x/L = 0.15$ in figure 4e is more accelerated than the velocity profile at $x/L = -0.05$ in Figure 4d. No evidence of reverse flow is seen in the mean profile at $x/L = 0.15$. By $x/L = 0.25$, the flow has separated, with a relatively large region of negative mean flow. From $x/L = 0.25$ to $x/L = 0.35$, the magnitude of the

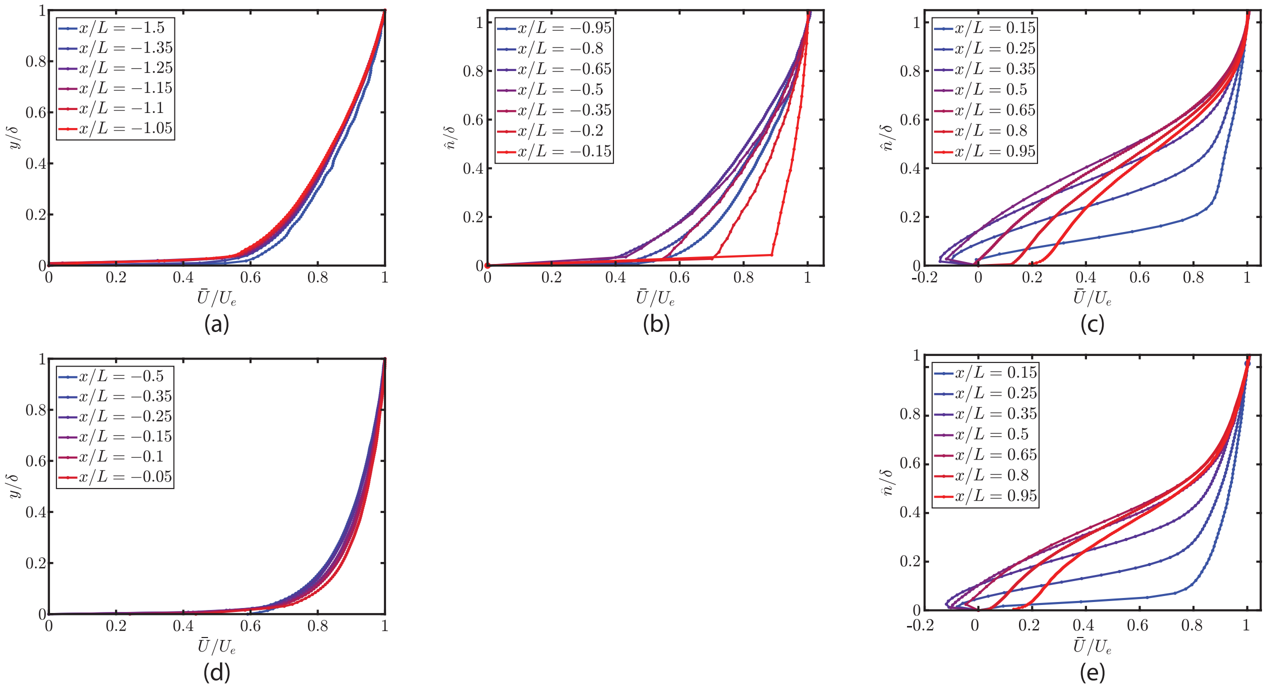

Figure 4. Evolution of mean streamwise velocities for (a)-(c) bump and (d)-(e) ramp.

reverse flow increased and the wall-normal extent of reverse flow also increased. The magnitude of reverse flow decreased from $x/L = 0.5$ to $x/L = 0.65$. At $x/L = 0.8$, the turbulent boundary layer shows signs of reattachment. The flow continues to accelerate near the wall from $x/L = 0.8$ to $x/L = 0.95$ and an inflection point is present at both locations.

Comparing the mean velocity profiles in the flat plate region of the bump and the ramp, in figures 4a and d, shows stark differences in the inflow conditions. At the same locations, the streamwise velocity profiles on the flat plate upstream of the ramp are much fuller compared to the bump profiles. This indicates the turbulent boundary layer has been accelerated by a mild FPG present over a large spatial extent upstream of the ramp. However, the upstream facing curvature of the bump yields a strong local FPG that generates a much fuller velocity profile at $x/L = -0.15$ in figure 4b, than any profile observed in the ramp. At the earliest streamwise location plotted in the strong APG region of both geometries, $x/L = 0.15$, in figures 4b and e, a very small mean reversed flow region is observed for the bump but not for the ramp. Furthermore, at this location farther away from the wall, the velocity profile for the bump is less full than the ramp. The local geometry is matched between the bump and ramp in Figures 4a and e, so the differences observed in the separation and reattachment locations are presumably due to the incoming flow differences. The turbulent boundary layer that encountered the ramp experienced a mild FPG over a long region of its development and then a localized FPG in the region of Figure 4d, while the boundary layer that encountered the bump experienced a ZPG over its development, with a much stronger and more localized FPG and curvature effect in its upstream facing half (Figure 4b).

To further quantify the different separation and reattachment behavior in the regions with strong APG in both geometries, the backflow percentage is plotted in figure 5. The backflow percentage, $1-\gamma$, is the percentage of time that reverse flow occurs and is calculated at each spatial location. Backflow percentage is calculated to understand the stage of separation of the TBL, as described by Simpson (1989). Both the ramp and bump at $x/L = 0.35$ have backflow around 85% of the time, meaning the TBL is fully detached. The downstream region of the bump experienced a larger backflow percentage at earlier streamwise positions, with around 55% backflow at a streamwise position of $x/L = 0.15$ whereas the ramp only experienced a backflow percentage of 30% at the same location. However, the flow remains detached longer for the ramp. The maximum backflow percentage at the streamwise position of $x/L = 0.65$ is 58% for the bump and 67% for the ramp. Furthermore, at the next streamwise location, the maximum backflow percentage is 23% for the bump and 41% for the ramp, demonstrating that the backflow percentage for the ramp remained higher farther downstream. For the last streamwise location, the backflow percentage for the ramp is 15% while the bump drops to 8%. The wall-normal extent of reverse flow events is larger for the bump, with backflow events occurring as high as $\hat{n}/\delta = 0.5$. Meanwhile, the wall-normal extent of reverse flow events for the ramp has backflow events only up to a wall-normal height of 0.45. Overall, this suggests the detachment point is slightly earlier for the bump. However, the area with higher backflow percentage is larger for the ramp.

A more accelerated boundary layer would be expected to yield a separation point that is farther downstream, potentially suggesting that the mild but consistently held FPG of the ramp's boundary layer was ultimately more impactful on the boundary layer's susceptibility to separation than the rapidly applied, very strong FPG of the upstream facing half of the bump. However, other factors including the influence of the Reynolds number and the boundary layer thickness may also have influenced the separation characteristics, requiring further inquiry and motivating future work.

Conclusion

The effects of pressure gradient history on the evolution of a turbulent boundary layer were evaluated experimentally

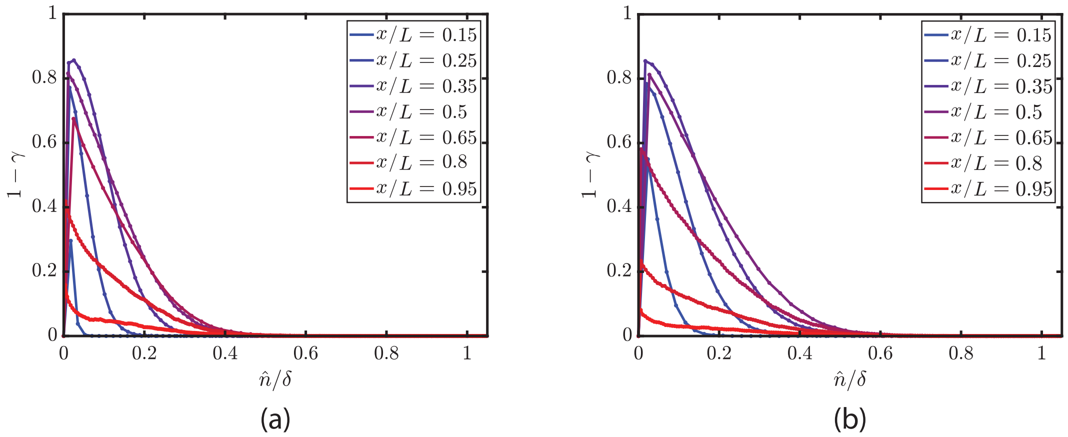

Figure 5. Backflow percentage in the strong APG region of (a) the bump and (b) the ramp

in a turbulent boundary layer wind tunnel at the University of Illinois Urbana-Champaign. Two different pressure gradient histories were imposed through a bump and downward facing ramp downstream of a flat plate. The difference in pressure gradient histories lead to varying in-flow conditions into the strong APG region of the bump and the ramp. The separation behavior of the turbulent boundary layer in the strong APG region is similar for both geometries however separation and detachment occurs at later streamwise positions for the ramp.

REFERENCES

Badri Narayanan, MA. & Ramjee, V. 1969 On the criteria for reverse transition in a two-dimensional boundary layer flow. *Journal of Fluid Mechanics* .

Balin, R. 2016 Physics and modeling of turbulent boundary layer flows under strong pressure gradients. PhD thesis, University of Colorado Boulder.

Balin, R. & Jansen, K.E. 2021 Direct numerical simulation of a turbulent boundary layer over a bump with strong pressure gradients. *Journal of fluid mechanics* .

Baskaran, V., Smits, A. & Joubert, P. 1987 A turbulent flow over a curved hill part 1. *Journal of Fluid Mechanics* .

Bourassa, C. & Thomas, F. O. 2009 An experimental investigation of a highly accelerated turbulent boundary layer. *Journal of Fluid Mechanics* .

Dixit, S. & Ramesh, O. 2010 Large-scale structures in turbulent and reverse-transitional sink flow boundary layers. *Journal of Fluid Mechanics* .

Gray, P., Thomas, F., Corke, T., Gluzman, I., Lakebrink, M. & Straccia, J. 2023 Experimental and computation evaluation of smooth-body separated flow over boeing bump. *AIAA Aviation 2023* .

Kline, S. J., Reynolds, W. C., Schraub, F. A. & Runstadler, P. W. 1967 The structure of turbulent boundary layers. *Journal of Fluid Mechanics* .

Monty, J.P., Harun, Z. & Marusic, I. 2011 A parametric study of adverse pressure gradient turbulent boundary layers. *International journal of heat and fluid flow* .

Na, Y. & Moin, P. 1998 Direct numerical simulation of a separated turbulent boundary layer. *Journal of fluid mechanics* .

Nagano, Y. & Tagawa, M. Tsuji, T. 1993 Effects of adverse pressure gradients on mean flows and turbulent statistics in a boundary layer. *Turbulent Shear Flows 8* .

Parthasarathy, A. 2023 Turbulent boundary layers under complex spatial and temporal pressure gradient histories. PhD thesis, University of Illinois Urbana-Champaign.

Patrick, W. P. 1987 Flowfield measurements in a separated and reattached flat plate turbulent boundary layer. *NASA Contractor Report* .

Prakash, A., Balin, R., Evans, J. & Jansen, K. 2022 Wall-modeled large eddy simulations of a turbulent boundary layer over the boeing speed bump at re_l =2 million. *AIAA SciTech 2022* .

Schlatter, P. & Orlu, R. 2010 Assessment of direct numerical simulation data of turbulent boundary layers. *Journal of fluid mechanics* .

Simpson, R. 1989 Turbulent boundary-layer separation. *Annual review of fluid mechanics* .

Slotnick, J., Khodadoust, A., Alonso, J., Darmofal, D., Gropp, W., Lurie, E. & Mavriplis, D. 2014 Cfd vision 2030: A path to revolutionary computation aerosciences. *NASA Reports* .

So, R. 1975 Experiment on turbulent boundary layers on a concave wall. *Aeronautical Quarterly* .

So, R. & Mellor, G. 1973 Experiement on convex curvature effects in turbulent boundary layers. *Journal of Fluid Mechanics* .

Sreenivasan, K R 1982 Laminarescent, relaminarizing and retransitional flows. *ACTA Mechanica* **44**, 1–48.

Uzun, A. & Malik, M. 2022 High-fidelity simulation of turbulent flow past gaussian bump. *AIAA* **60**.

Vila, S., Vinuesa, R., Discetti, S., Ianiro, A. Schlatter, P. & Orlu, R. 2020 Experimental realisation of near-equlibrium adverse-pressure gradient turbulent boundary layers. *Experimental thermal and fluid science* .

Vineusa, R., Orlu, R. & Schlatter, P. 2016 On determining characteristics length scales in pressure gradient turbulent boundary layer. *Journal of Physics: Conference Series* .

Vinuesa, R., Orlu, R., Vila, C., Ianiro, A., Discetti, S. & Schlatter, P. 2017 Revisiting history effects in adverse-pressure-gradient turbulent boundary layers. *Flow, Turbulence Combustion* **99**, 565–587.

Volino, R. 2020 Non-equlibrium development in turbulent boundary layers with changing pressur gradients. *Journal of Fluid Mechanic* .

Webster, D., DeGraff, D. & Eaton, J. 1996 Turbulence characteristics of a boundary layer over a two-dimensional bump. *Journal of Fluid Mechanics* .

Wu, W., Menevaeu, C. & Mittal, R. 2020 Spatio-temporal dynamics of turbulent separation bubbles. *Journal of Fluid Mechanics* .